European Journal of Pharmaceutics and Biopharmaceutics 74 (2010) 109–119

Contents lists available at ScienceDirect

European Journal of Pharmaceutics and Biopharmaceutics

journal homepage: www.elsevier.com/locate/ejpb

Research paper

Magnetic resonance imaging and X-ray microtomography studies of a gel-forming tablet formulation

P.R. Laity [a,*], M.D. Mantle [b], L.F. Gladden [b], R.E. Cameron [a]

[a] Department of Materials Science and Metallurgy, University of Cambridge, Cambridge, UK
[b] Department of Chemical Engineering, University of Cambridge, Cambridge, UK

ARTICLE INFO

Article history:
Received 23 May 2008
Accepted in revised form 22 June 2009
Available online 27 June 2009

Keywords:
X-ray microtomography (XμT)
Magnetic resonance imaging (MRI)
Tablet
Swelling
Hydroxypropyl-methyl-cellulose (HPMC)
Gel-forming

ABSTRACT

The capabilities of two methods for investigating tablet swelling are investigated, based on a study of a model gel-forming system. Results from magnetic resonance imaging (MRI) were compared with results from a novel application of X-ray microtomography (XμT) to track the movements of embedded glass microsphere tracers as the model tablets swelled. MRI provided information concerning the movement of hydration fronts into the tablets and the composition of the swollen gel layer, which formed at the tablet surface and progressively thickened with time. Conversely, XμT revealed significant axial expansion within the tablet core, at short times and ahead of the hydration fronts, where there was insufficient water to be observed by MRI (estimated to be around 15% by weight for the system used here). Thus, MRI and XμT may be regarded as complementary methods for studying the hydration and swelling behaviour of tablets.

© 2009 Elsevier B.V. All rights reserved.

1. Introduction

Tablets are a very popular, versatile and widely used means of administering drugs [1]. While the role of the pharmacologically active ingredient is self evident, the excipients can also affect the efficacy of the formulation [2,3]. The excipients may help to stabilise the drug and control its dissolution within the alimentary tract, but are rarely simple diluents or bulking agents.

Gel-forming excipient mixtures offer a convenient method for producing tablets that exhibit sustained release of drug over typically 8–24 h [2–6]. This may be important for several reasons: a reduced frequency of administration may assist in compliance; the drug concentration may remain at a therapeutic level for longer; avoiding the concentration spikes associated with 'burst-release' formulations may prevent adverse side-effects.

Various hydrophilic polymers have been investigated as the basis for gel-forming, sustained-releasing tablets, of which hydroxypropyl-methyl-cellulose (HPMC) currently appears to be amongst the most useful [6]. When swallowed, these tablets rapidly form a hydrated surface gel layer, which controls the subsequent water ingress and resists rapid disintegration. Thus, the rate of drug release is controlled by a number of inter-related factors such as the rate of water diffusion and tablet swelling; thickness and dissolution or erosion of the gel layer, drug solubility in and diffusion through the gel layer, which depend on the initial 'dry' composition of the excipients used [5–12]. Consequently, the quantity of drug, $Q(t)$, released is frequently observed to follow a power-law time dependence [2]:

$$Q(t) = kt^{\alpha} \tag{1}$$

where k is a constant, and the exponent can indicate diffusion behaviour ranging from sub-Fickian ($\alpha < 0.5$) to 'case II' ($\alpha = 1$). It should be noted that, while $Q(t)$ may follow a simple mathematical relationship, this arises from considerably complex underlying processes.

Experimental studies of gel-forming tablets present significant technical challenges. The simplest method involves measuring the rate of drug released over a period of time; however, this reveals little concerning the underlying behaviour of the tablet or release mechanisms. More detailed information can be obtained from imaging studies, in which the tablet behaviour is observed directly. From a mechanistic perspective, the whole tablet should be studied *in situ*, with the minimum of manipulation, to avoid artificial disruption of the gel layer, but this imposes constraints on the spatial resolution and acquisition time for each measurement. It may be noted, however, that swallowing produces a somewhat different situation since peristalsis and contact with the gut or stomach contents may mechanically disrupt the gel layer.

Of the candidate methods currently available, magnetic resonance imaging (MRI) has proved very useful and has been used

* Corresponding author. Pfizer Institute for Pharmaceutical Materials Science, Department of Materials Science and Metallurgy, University of Cambridge, Pembroke Street, Cambridge CB2 3QZ, UK. Tel.: +44 1223 767059; fax: +44 1223 334567.
E-mail address: prl28@cam.ac.uk (P.R. Laity).

0939-6411/$ - see front matter © 2009 Elsevier B.V. All rights reserved.
doi:10.1016/j.ejpb.2009.06.014

extensively [13–29]. Nevertheless, there may still be problems with issues such as chemical selectivity and sample presentation. Consequently, it is desirable to have additional methods that may be used in comparison with MRI. For example, Adler and co-workers used confocal microscopy with fluorescent tracer particles to study tablet swelling [30]. This method was able to observe the progressive onset of swelling at successive points as the hydration front gradually penetrated into the tablet. Due to the constraints of confocal microscopy, however, it was only possible to study thin slices cut from tablets.

The work reported here used a novel combination of MRI and X-ray microtomography (XμT) to provide further insight into the swelling behaviour of the tablets. While MRI was able to observe water ingress and the formation of the surface gel layer, XμT provided information on the dynamic behaviour of the tablet during swelling, including those regions that were insufficiently hydrated to give an observable NMR signal.

1.1. Magnetic resonance imaging

MRI covers an extensive range of sophisticated and widely used techniques for studying the distribution and dynamics of selected species within a material, based on their nuclear magnetic resonance (NMR) effects. Detailed descriptions are given by Richardson et al. [13], Callaghan [31] Blümich [32] and others [33–37]; so, only the key points are summarised here.

Although useful NMR signals can be obtained from isotopes of several elements, the hydrogen nucleus, ^{1}H, is the most sensitive (excepting its radioactive isotope tritium) and consequently MRI is particularly useful for studying water and hydrogen-bearing organic materials. MRI can achieve full three-dimensional (3D) spatial resolution using orthogonal pulsed magnetic field gradients. It can also provide selectivity on the basis of diffusion and nuclear spin relaxation times, which are related to physical state and molecular motion. Quantitative measurements based on observed NMR intensities are possible; however, compensation for signal attenuation due to spin relaxation and diffusion is often needed, which requires more sophisticated pulse sequences and longer acquisition times.

MRI has been used to study the swelling behaviour of tablets based on HPMC [14–21] and other cellulose ethers [21], starch [22,23], xanthan [24] and other hydrophilic materials [25–29]. Imaging studies of HPMC by Rajabi-Siahboomi et al. [14] and Kojima et al. [15] indicated that the axial swelling was considerably greater than radial, which was attributed to stress relaxation within the tablet core. Malveau and co-workers [23] observed similar behaviour in starch tablets, which they attributed to granules becoming flattened during compaction and returning to spherical shape during swelling. More quantitative investigations of HPMC tablets, incorporating measurements of longitudinal and transverse relaxation times (T_1, T_2) and diffusion coefficients (D), are reported by Kojima and Nakagami [16], Fyfe and Blazek [17,18] and Baumgartner et al. [21]. The relationships between composition, T_2 and self-diffusion suggested a considerable interaction between water and the swelling HPMC, while T_1 relaxation profiles indicated progressive dilution of the HPMC across the surface gel towards bulk water.

Using *in situ* MRI measurements, Fyfe and Blazek [17] observed a square-root of time ($t^{1/2}$) relationship, for axial diffusion of water at 22 °C into HPMC, indicating Fickian diffusion. Fickian diffusion has also been inferred for water ingress into compacted xanthan powder [24], while case II (linear) diffusion has been reported for axial water penetration into starch tablets [22,23]. Kowalczuk et al. [19,20] investigated the radial swelling of HPMC tablets in dilute hydrochloric acid (pH = 2.0, to simulate the stomach) and water (pH = 6.0, to simulate the intestines). Using an experimental procedure that involved periodical removal of the medium from tablets, these authors observed Fickian water penetration at pH 6, but case II at pH 2. The penetration rate was also significantly faster at 37 °C than 25 °C. These observations indicate important effects of the swelling medium and tablet composition. Differences in tablet porosity and residual stress, as a consequence of compaction conditions and composition, may also occur.

1.2. X-ray microtomography

XμT is a non-destructive technique that generates a 3D map (reconstruction) of the specimen under examination, using a series of X-ray images (projections) obtained in different directions with respect to the specimen. Imaging represents the earliest use of X-rays, while the principles of tomography are well established. Advances in computing power, which is required for generating the 3D reconstructions, led to a rapid development in medical X-ray tomography over the past 30 years. Further advances in computers and X-ray detectors during the 1990s have facilitated the development of bench-scale XμT, with resolution in the order of a few micrometres. Comprehensive explanations of XμT are given by Baruchel et al. [38], Stock [39,40] and Kak and Slaney [41]; so, only a few key points are mentioned here.

Commonly, as in the present work, the imaging contrast in XμT arises from X-ray absorbance, which increases with the atomic number and mass density of the material. Consequently, XμT is very useful for examining cracks and voids within otherwise homogeneous materials or regions of different elemental composition. Other methods, based on scattering, fluorescence or phase-contrast, are also known [38–40], which can offer advantages in some cases but are generally limited to synchrotron X-ray sources.

In principle, it should be possible to establish quantitative relationships between the observed X-ray absorbance in the reconstruction and density or composition variations within the sample. Ideally, such measurements would be taken using a parallel beam of monochromatic illumination, which is feasible at a synchrotron source. However, the situation is generally made more difficult by the use of a cone- or fan-beam (to obtain geometric magnification) and polychromatic illumination (to overcome the limited photon flux) in bench-top XμT apparatus. In particular, the use of polychromatic illumination incurs variations of absorbance with photon energy, which leads to 'beam hardening'. The lower energy fraction of the light entering the object is absorbed preferentially, while the higher energy fraction is more penetrating. This can cause a false increase in the contrast close to the surface of the specimen, which can lead to erroneous variations in the density (or composition) in the reconstructed data.

1.3. Applications of XμT

XμT has been used extensively to study engineering materials [38–45], geological specimens [46,47], physiological samples and bio-materials [48–50]. By contrast, there has been relatively little work reported using XμT to study pharmaceutical systems. Sinka et al. [51] and Busignies et al. [52] used X-ray computed tomography to determine density distributions in pharmaceutical tablets; Ozeki et al. [53] compared dry-coated tablets; Yang and Fu [54] reported lead acetate staining as a means of marking microcrystalline cellulose for tabletting studies. Rigby et al. [55] recently reported studies of drug distribution in model tablets using two-dimensional X-ray microbeam imaging, but noted the possibility of 3D studies using XμT. No studies of the swelling or dissolution of pharmaceutical systems appear to have been reported previously.

By using both MRI and XμT (separately) to observe identical specimens, the present work demonstrated the potential of these

complementary methods for studying the 3D swelling behaviour of gel-forming tablets.

2. Materials and methods

Experiments were performed using a tablet composition similar to that reported by Williams et al. [11] as a reasonably fast gel-forming system. HPMC (Methocel K4M premium EP, Colorcon, UK, 40 g), microcrystalline cellulose (MCC, Avicel PH102, FMC Europe, 33.3 g) and lactose (Lactose New Zealand, 17.3 g) were placed in a plastic container and tumbled at 49 rpm for 1 h, using a Turbula mixer (Willy A Bachofen AG, Switzerland). Where required, portions of this masterbatch were removed and mixed for a further 15 min with glass microspheres (2% w/w, nominally 106–180 μm diameter). Portions of the appropriate mixture (0.4 ± 0.01 g) were made into flat-faced cylindrical tablets by single-sided compaction in a 13 mm diameter die (Specac Ltd. UK) and a hydraulic press, at 1 tonne (equivalent to 74 MPa) for 1 min. The tablet thickness, measured using callipers with a vernier scale, was 2.75 ± 0.10 mm.

All swelling experiments were performed in triplicate, in phosphate-buffered saline (PBS) solution, containing 0.137 M NaCl, 0.0027 M KCl and 0.01 M phosphate buffer, at pH 7.4. A model tablet was mounted on a thin, tubular support in the centre of a poly(-methyl methacrylate) specimen vial, as shown in Fig. 1a, and immersed in PBS solution at ambient temperature.

The use of relatively large tablets restricted the swelling rate and reduced the requirements for rapid imaging acquisitions and high spatial resolution. Consequently, these tablets were only slightly smaller than the inside diameter of the specimen vial, which fitted snugly into the MRI imaging coil and just remained within the field of view of the XμT. This optimised observations of axial swelling, while radial swelling generally appeared constrained by gel bridging onto the vial wall and has been ignored in the present work.

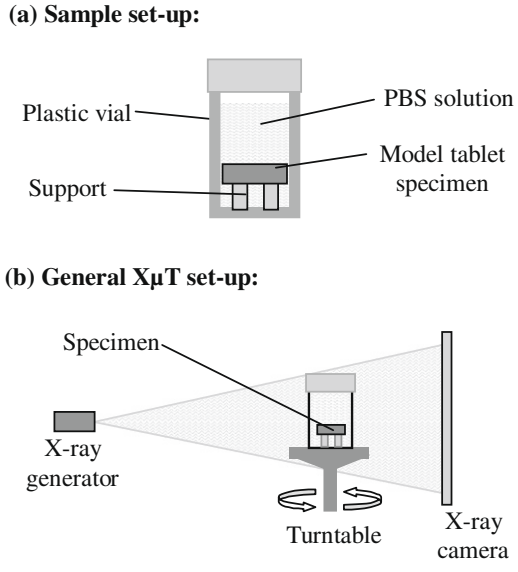

Fig. 1. Experimental set-up for swelling experiments.

2.1. XμT swelling studies

XμT was performed using a model 1072 apparatus (Sky-Scan, Belgium) equipped with a 1024 × 1024 pixel camera and a polychromatic, sealed tungsten source, producing cone-beam illumination. The vial, containing a model tablet incorporating glass microspheres in PBS solution, was mounted in the XμT, as shown in Fig. 1b. Images were acquired at 15× magnification, equivalent to a pixel size of 18.3 μm and a total field of view of 18.8 mm × 18.8 mm; the source was set at 100 kV and 98 μA, and a 0.5-mm aluminium filter was used. Acquisitions were performed over 180°; step size, detector gain, exposure time and frame-averaging were adjusted, depending on the desired acquisition time. Relatively clear but slow acquisitions (approximately 1 h) were used for dry tablets; faster acquisitions (down to approximately 10 min) were used for rapidly changing samples near the start of the swelling experiments. Typical instrument settings are shown in Table 1.

The specimens remained in the XμT apparatus throughout the duration of each swelling experiment, which established a common 3D Cartesian co-ordinate system, with the tablet compression direction as the (vertical) *z*-axis, as shown in Fig. 1c. Glass microspheres to be tracked were selected at different starting positions within the tablet. The *x*- and *y*- co-ordinates of each microsphere were obtained from the position within the reconstructed cross-section slice; the *z*-co-ordinate was obtained from the slice number within the vertical stack of (up to 1024) reconstructed images (also spaced at 18.3 μm intervals). Hence, the movement of glass markers could be tracked from one acquisition to the next. This was similar to the methodology devised by Aydin et al. [56] and subsequently employed by Eiliazadeh et al. [57] to study tablet compaction, except that the continual changes caused by swelling required a compromise between speed and clarity in the imaging conditions. Changes in tablet shape and size could then be observed in terms of the distances between glass microspheres.

2.2. MRI swelling studies

All ^{1}H imaging experiments were performed on a Bruker Biospin DMX 300 spectrometer operating at a ^{1}H frequency of 300.13 MHz. ^{1}H excitation and detection were achieved using a 15 mm diameter birdcage radio-frequency coil. Spatial resolution was achieved using an actively shielded gradient system capable of producing a maximum magnetic field gradient (G), in all three Cartesian directions (x, y and z), of 1 T m^{-1}. A slice of 4.0 mm thickness was excited in the zx plane (see Fig. 1c). The field of view was 15.0 mm in both the read (z) and phase (x) directions. For each image, 128 × 32 data points were acquired in the read and phase directions, respectively, yielding an in-plane pixel resolution of 469 μm (horizontal) by 117 μm (vertical, i.e. tablet axial direction).

Spatially resolved data were acquired by combining an inversion-nulling filter with a slice-selective variant of the multiple-

Table 1
Summary of instrument settings for XμT acquisitions.

Step size (°)	Number of frames per step	Gain	Frame exposure time (s)	Approximate acquisition time (min)
0.9	2	1.0	6.2	60
0.9	1	1.0	6.2	30
1.8	1	1.0	6.2	18
1.8	1	2.0	3.1	10

echo Carr–Purcell–Meiboom–Gill (CPMG) pulse sequence [31,32], in the form: $P180_x$-τ-$P90_x$-(t_d-$P180_y$-t_d-echo-)$_n$-t_R. It was found that an inversion delay (τ) of 2.04 s effectively suppressed the signal from bulk water. The pulse delay (t_d) was 1.26 ms and the recycle time (t_R) was 9.0 s. The total acquisition time for a set of 16 echoes (consisting of two averages) was 9.5 min.

In order to visualise the swelling behaviour, semiquantitative images were extracted from the first echo (at echo time $t_E = 2t_d = 2.52$ ms) of the sequence for each phase-encoding step. Estimates of the transverse relaxation for the observable species (i.e. water and any sufficiently mobile excipients) were obtained by analysing the subsequent changes in echo intensities.

Spatially unresolved (i.e. without imaging gradients) 'calibration' experiments were also performed in order to understand the relationships between water content and the observed MRI intensities better. Small quantities of distilled water (measured to ± 0.0003 g) were added to tablets individually sealed inside plastic sample vials, which were refrigerated and allowed to equilibrate for 50 days. Uniform water distributions within the specimens were assumed although imaging to confirm this was prevented by shape changes during swelling (i.e. cockling at low water levels, sagging or collapse at higher water levels). The overall signal strengths were estimated using a single (Hahn) echo sequence with relatively short echo times ($t_E = 0.2$ and 0.4 ms) and performing a linear extrapolation to $t_E = 0$. Longitudinal (T_1) relaxation measurements were taken using an inversion recovery sequence. Transverse relaxation (T_2) measurements were taken using a CPMG pulse sequences (without inversion-nulling). Additional diffusive losses, due to magnetic susceptibility differences within the specimens, were evaluated by comparing T_2 from CPMG experiments with effective $T_{2(eff)}$ results from Hahn echoes over a range of t_E values between 0.2 and 120 ms.

3. Results

3.1. MRI imaging studies

Images of tablet cross-sections (i.e. x–z plane) at various stages during swelling are presented in Fig. 2. In general, the intensity of the nth echo, $M(n)$, was expected to depend on water content, through changes in diffusivity (D) and relaxation times as well as the concentration of (observable) hydrogen atoms [31,32]:

$$M(n) = M_0 \cdot \exp\left\{-\frac{D}{12}\gamma^2 G^2 t_E^3 n\right\} \cdot \exp\left\{-\frac{nt_E}{T_2}\right\} \cdot \left\{1 - B \cdot \exp\left(\frac{-\tau}{T_1}\right)\right\} \quad (2)$$

where M_0 is proportional to the population of observable spins (due to water and any sufficiently mobile excipient species), B is a constant (=2.0 expected) and γ is the gyromagnetic ratio for protons (=0.2675 × 10^9 rad s^{-1} T^{-1} [32]).

The first bracketed term shows that diffusive attenuation increases rapidly with echo time and magnetic field gradients. Based on G and t_E used in the imaging experiments, with $n = 1$ for the first echo, the first exponential term in Eq. (2) was estimated to be 0.82 for pure water and closer to 1 for the slower diffusion expected within gel at low hydration. As previously demonstrated [58], however, heterogeneous materials can generate 'adventitious' field gradients due to differences in magnetic susceptibilities between the various phases, which can give rise to further diffusional losses. Hence, in order to minimise attenuation due to diffusion and T_2 relaxation (the second exponential term in Eq. (2)), it was important to collect the imaging data with t_E as short as possible. The value of $t_E = 2.52$ ms chosen for this work was the shortest practicable for imaging experiments, with the apparatus used.

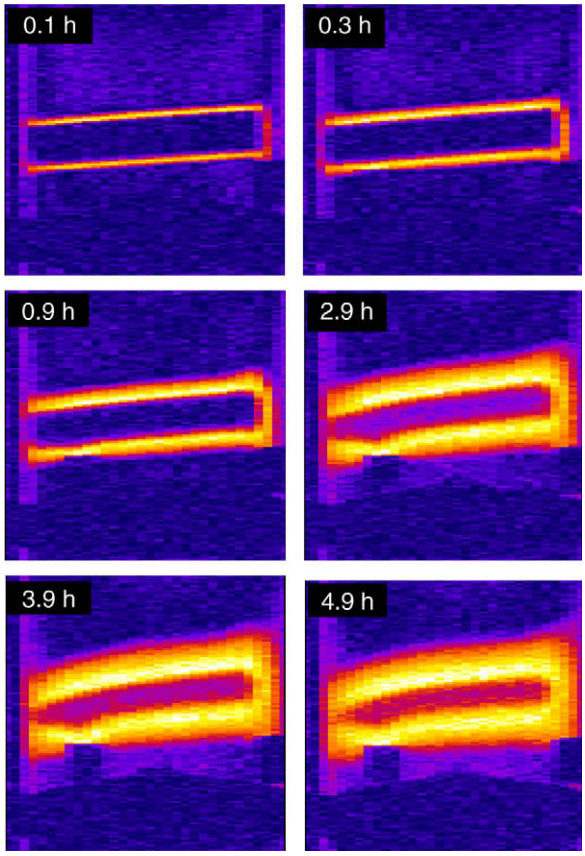

Fig. 2. Intensity maps of diametral sections from first echoes of MRI acquisitions at selected times (mid-points of acquisitions), arbitrary, linear intensity scale: lighter colour indicates stronger signal. (For interpretation of the references to color in this figure legend, the reader is referred to the web version of this paper.)

Dry excipients, with short T_2, produced no observable signal. Ingress of water into the tablet was revealed as a rise in intensity, as T_2 increased with swelling. The signal from bulk liquid was effectively suppressed by an inversion-nulling filter, represented by the third exponential term in Eq. (2). Hence, the gel–water interface was revealed by an increase in signal strength, as the swollen or dissolved excipients decreased T_1, which reduced the effect of the inversion-nulling.

A small but significant signal was observed from the edges of the tablet, in the first image (at 0.1 h), which suggested that a thin surface gel layer formed relatively quickly. This was supported by other observations that the tablet surface rapidly (i.e. within 1 min) became sticky, following immersion in PBS solution. Subsequent observations revealed that the gel layer thickened by the hydration front advancing at roughly constant speed towards the tablet centre and progressive swelling towards the bulk liquid.

3.2. Composition, relaxation and signal strength

It is well known that T_1 and T_2 are strongly affected by composition; indeed, previous workers used relaxation measurements to study the composition of the gel layer [17,21]. While we were less interested in the gel composition, in the present work, it was important to establish the composition limits corresponding to the (inward) advancing hydration front and the (outer) gel–liquid interface.

Results from T_1 measurements are shown in Fig. 3. Examples of recovery curves using a spin-inversion pulse sequence are shown in Fig. 3a, for three water levels. In each case, the data were found to closely fit a model in the form:

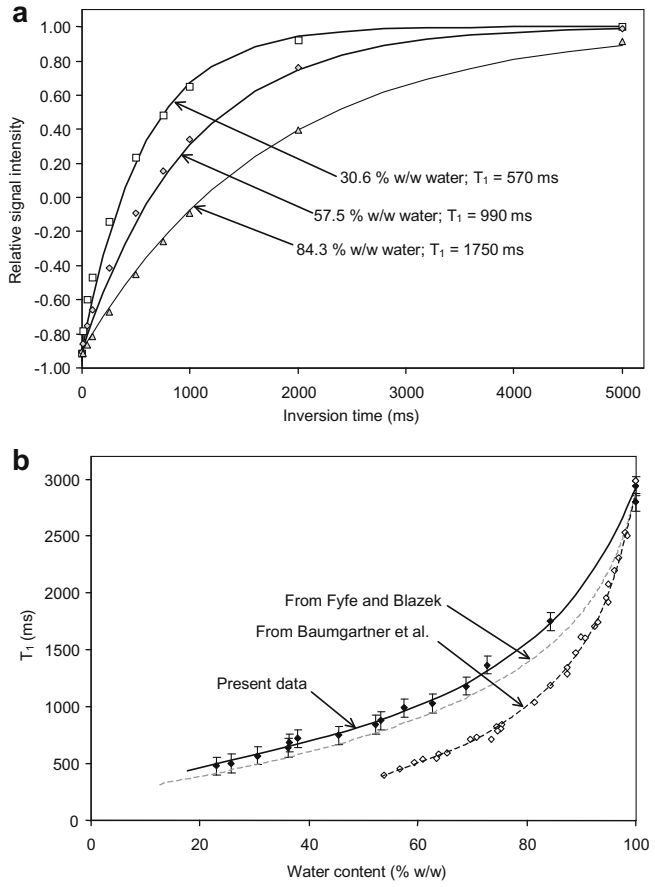

Fig. 3. Longitudinal relaxation measurements; (a) selected inversion recovery plots, continuous lines indicate expected single-exponential recovery with T_1 values shown and (b) variation of T_1 with water content (data from Fyfe and Blazek [17] and Baumgartner et al. [21] shown for comparison).

$$\frac{M(\tau)}{M_0} = 1 - B\exp\left(\frac{-\tau}{T_1}\right) \tag{3}$$

where B was evaluated as 1.9. It may be noted that theory predicts a value of $B = 2.0$. The departure from this in the present work may be attributable to imperfections in the inversion pulse; however, similar effects can be produced by a mixture of phases with different T_1 values.

The relationship between composition and T_1 measured in the present work is shown in Fig. 3b, where the error bars represent the maximum uncertainty from curve fitting the inversion data. The recent results are also compared with previously published data. At first sight, the present results appeared to agree better with those from Fyfe and Blazek [17]. However, as Baumgartner et al. [21] reported that the relationship between T_1 and composition was also sensitive to the excipient type, the present results, based on a mixed system, should not be expected to agree closely with the previously published work using single excipients.

The composition limit corresponding to the gel–liquid interface can be estimated from the change in T_1 with water content, shown in Fig. 3b. Using the inversion-nulling filter, less than 5% of the (unsuppressed) signal from bulk PBS solution was observable. (This produced the feint background observable at 0.1 h swelling, in Fig. 2.) A doubling in this signal strength was expected for $T_1 = 2.73$ s, corresponding to 98% w/w water, which appeared to be a reasonable estimate for the observable composition at the gel–liquid interface.

Conversely, T_1 decreased to below 600 ms, for gel containing less than 30% w/w water. Under these conditions, signal suppression due to inversion-nulling was estimated to be less than 10%. Hence, the inversion-nulling effect could be neglected for imaging regions with lower water levels, close to the advancing hydration fronts.

As noted previously, further signal attenuation can result from diffusion in 'adventitious' field gradients caused by magnetic susceptibility differences [58]. CPMG measurements are largely unaffected by this, due to the re-focusing effects of the P180$_y$-pulses between echoes. Effectively, the attenuation is described by Eq. (2) with increasing values of n for successive echoes. By contrast, $n = 1$ for the Hahn pulse sequence, but increasing values of t_E give stronger diffusional attenuation. Consequently, Hahn experiments give 'effective' $T_{2(eff)}$ values, which combine relaxation and diffusive losses, while CPMG results are closer to pure T_2.

Measurements using CPMG and Hahn experiments are compared in Fig. 4a and b for gels at two hydration levels. In each case, the intensities appeared to be well represented by a single-exponential decay, in the form:

$$\frac{M(t_E)}{M_0} = \exp\left(\frac{-t_E}{T_{2(eff)}}\right) \tag{4}$$

where $T_{2(eff)}$ depended on the measurement method. The fit was very good at higher water levels, suggesting that the samples were effectively homogeneous, but less good at lower water levels where the attenuation was faster and the overall signal intensity was less. In each case, the attenuation was faster in Hahn experiments compared with CPMG sequences, indicating significant diffusive losses.

Changes in $T_{2(eff)}$ with water content and measurement method are shown in Fig. 4c; again, the error bars represent the maximum uncertainty from fitting the relaxation data. In spite of differences between the excipient systems used, the present data compared well with previously published results by Baumgartner et al. [21] (using CPMG) and Fyfe and Blazek [17] (using Hahn echoes).

Clearly, the composition limit corresponding to the advancing hydration front depended on three factors linked to the water content: the overall concentration of hydrogen atoms, T_2 relaxation and diffusive losses before the first echo could be collected. This is demonstrated in Fig. 5. The upper curve shows the intensities without relaxation or diffusional losses, which were estimated by extrapolation to $t_E = 0$, from Hahn echoes at 0.1 and 0.2 ms, for a fixed amount of gel containing between 0% and 70% hydration. This curve decreased towards lower hydration levels, but remained above zero since the dry excipients also contained hydrogen atoms. The lower curve shows the expected intensities for imaging at $t_E = 2.52$ ms, after allowing for inversion-suppression, relaxation and diffusional losses. In particular, changes in T_1 with water content were as shown in Fig. 3b, for an inversion-nulling filter with $\tau = 2.04$ s; Hahn $T_{2(eff)}$ results were used, which incorporated the effects of T_2 relaxation and magnetic susceptibility differences on diffusional losses. This curve peaked around 65% water, due to the dominant inversion-suppression at higher water levels and faster T_2 relaxation at lower water levels. Significantly, the intensity approached zero at low water levels and fell below the level of background 'noise' estimated from the imaging experiments. An observable signal at twice this background noise level was predicted around 15% w/w water.

It must be assumed that the calibration experiments (with specimens equilibrated over 50 days) were representative of dynamic swelling behaviour, with much shorter timescales (minutes to hours). This may not be entirely correct, considering the rôle of polymer relaxation during swelling. Nevertheless, it appears reasonable that the gel regions observed in Fig. 2 corresponded to hydration levels between roughly 15% and 98% w/w water.

3.3. Composition changes during swelling

Typical changes in (first echo) signal intensity across a partially swollen specimen (at 1.9 h) are shown in Fig. 6a. Echo decay measurements using a CPMG sequence at selected locations within this

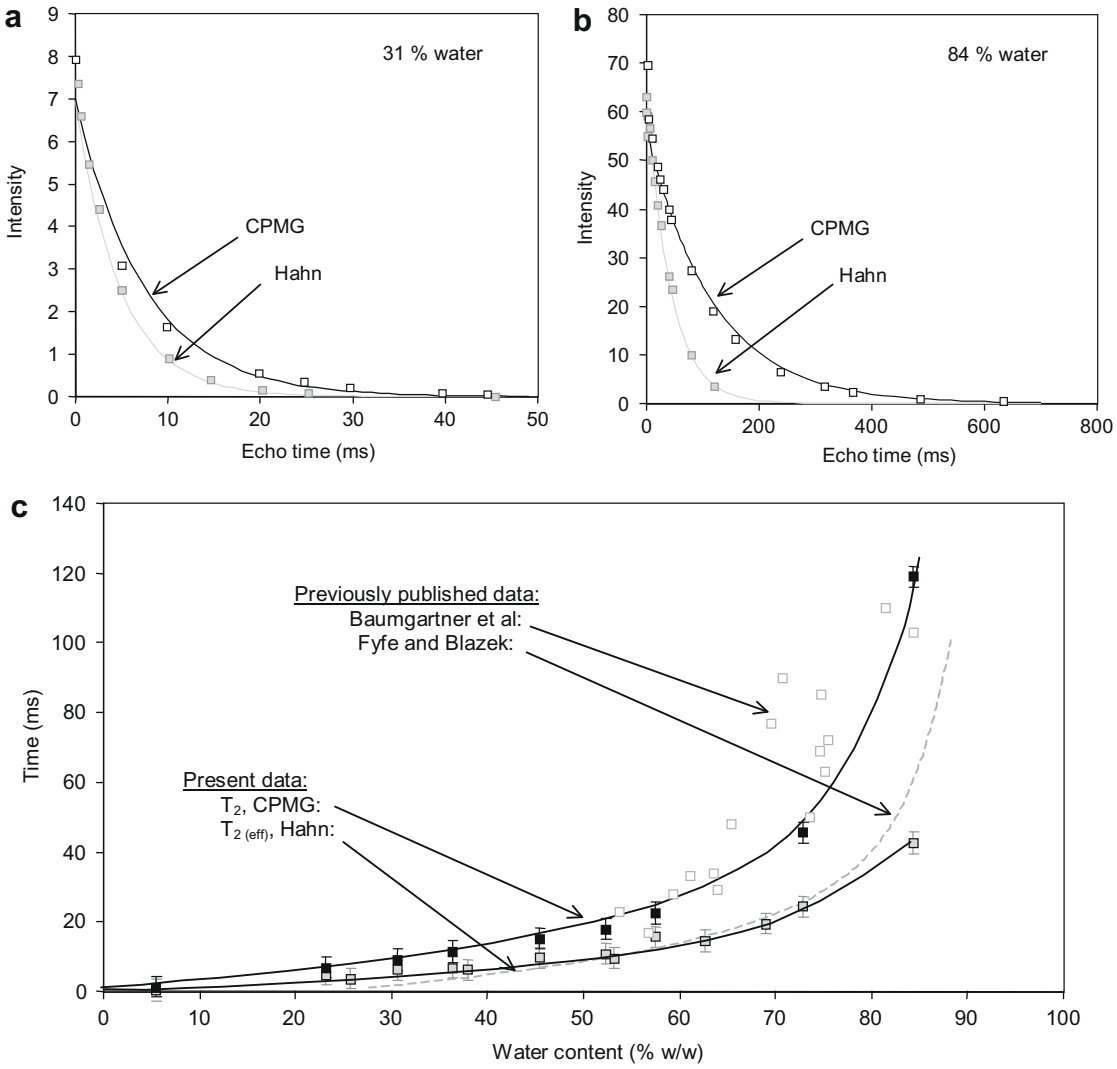

Fig. 4. T_2 and effective T_2 relaxation measurements; CPMG and Hahn echo decay plots, continuous lines indicate expected single-exponential models for (a) 31% w/w water gel; (b) 84% w/w water gel; and (c) variation of $T_{2(eff)}$ with water content, (data from Fyfe and Blazek [17] and Baumgartner et al. [21] shown for comparison).

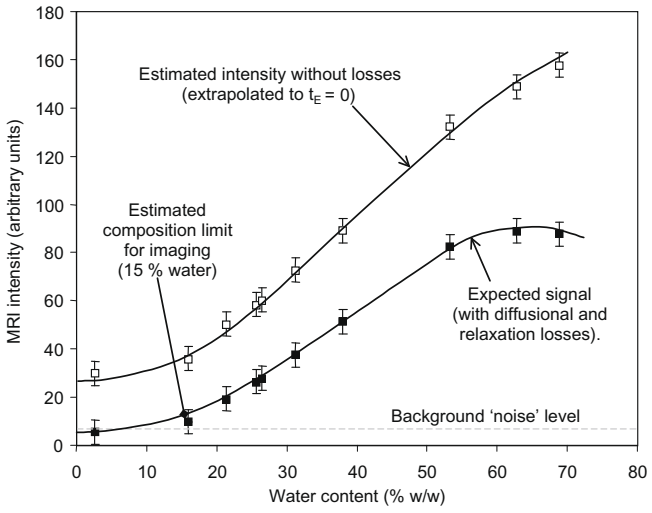

Fig. 5. Estimate of low water detection limit from effects of water content on hydrogen atom concentration, transverse relaxation rate and diffusive losses.

specimen are shown in Fig. 6b. As expected, the relaxation was considerably faster towards the advancing hydration fronts (points E and F) compared with closer to the gel–liquid interface (points A and B), due to the decrease in hydration between the gel–liquid interface and the tablet core. Point F represented the practical limit for T_2 measurement close to the hydration front, since successive echoes from the next pixel towards the tablet core rapidly became dominated by noise. Significantly, the value of $T_{2(eff)}$ = 5.3 ms measured at point F corresponded to 17% w/w water in the gel, which agreed well with the expectation discussed in the previous section.

Changes in $T_{2(eff)}$ values across the specimen, where there was sufficient signal intensity for successful measurements, are shown in Fig. 6c. Essentially, the gels above and below the tablet core appeared symmetrical, with $T_{2(eff)}$ increasing linearly from the hydration fronts outwards.

Fig. 6d presents estimates of water content obtained from the data in Fig. 6c, using the relationship shown in Fig. 4b. The water content appeared to rise rapidly behind either hydration front, then more slowly towards the gel–liquid interfaces. These results were highly suggestive of case II diffusion, which is embodied by a narrow region where solvent concentration and diffusion increase steeply, followed by a region of approximately constant composition [59]. Since movement is largely governed by the rate of polymer swelling at the front, it is predicted that the hydration fronts should advance at constant speed – in line with MRI observations on the present system.

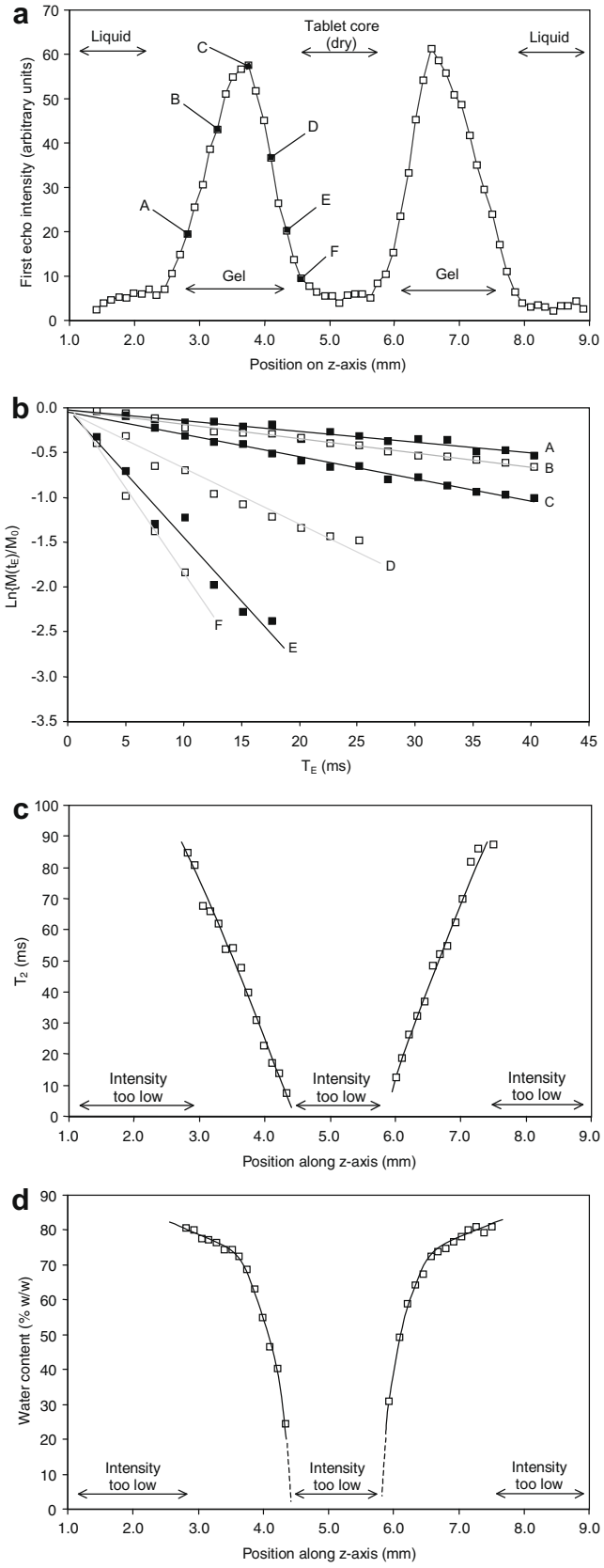

Fig. 6. (a) Variations of first echo intensity along *z*-axis (arbitrary units) after 1.9 h swelling; (b) T_2 measurements using CPMG pulse sequence, at selected locations indicated in (a) across gel layer; (c) variations in T_2 across specimen (where sufficient intensity was obtained); (d) water content estimated from data in (c).

3.4. XμT studies

XμT images of a dry tablet are presented in Fig. 7. The walls of the sample vial are clearly visible as vertical stripes at either side of the projection image (Fig. 7a); the tablet appears as a transparent disk, mounted on a narrow plastic support. The irregular dark mass was 'Blue-tack' adhesive, to hold the tablet on the support; this was only required for dry samples, since the tablet surface rapidly (<1 min.) became sticky when immersed in PBS solution. The glass microsphere tracer particles may be observed by close examination of the projection image, but are quite clear as small dark dots in the reconstructed (horizontal and vertical) cross-sections (Fig. 7b and c, respectively).

Measurements from the reconstructed cross-sections gave a tablet thickness of 2.8 mm and diameter of 13.0 mm, in good agreement with measurements using callipers.

Selected XμT projection images of a tablet at various stages during a swelling experiment are shown in Fig. 8. A short delay (approximately 2 min) occurred while the tomograph sample hatch and radiation shielding were closed, prior to starting the first acquisition. Combined with the finite acquisition time (a minimum of 10 min in the present work), this produced a 'blind spot' of approximately 7 min (to the mid-point of the first acquisition) at the start of the swelling experiment. In principle, this could be overcome using XμT of the dry tablet prior to adding PBS solution. In practice, however, addition of the PBS solution generally caused some sample movement, which prevented accurate registration of the starting positions of the selected markers. Instead, the starting positions were estimated by extrapolating the observable data.

Weak X-ray contrast between the tablet, the plastic support and the PBS solution generally limited the observable detail in the collected profiles (not shown). This was most severe when the imaging conditions were selected for rapid acquisitions, during the early stages of swelling. Nevertheless, considerably more detail was observable in the reconstructed images, which also improved when longer acquisitions were possible.

In addition to showing the positions of the glass microspheres, the vertical reconstructed cross-sections revealed the presence of regions of light contrast (i.e. lower X-ray absorbance), which started by outlining the tablet profile but increased in thickness and moved towards the tablet core as swelling progressed. In general, lower X-ray absorbance is associated with lighter elements or lower mass density [38–41]. In the present studies, however, no mechanism involving the former could be envisaged; hence, the light contrast indicated regions of low mass density. This may be attributed to the formation of microscopic (i.e. smaller than the pixel size, 18.3 μm) bubbles in the swollen gel. Bubble formation during swelling has been reported previously by Melia et al. [60] and has been attributed to air that was entrained in pores between or within excipient granules during compaction.

Glass microsphere markers starting at different locations within the tablet were chosen and their co-ordinates were obtained manually from the 'stacks' of horizontal reconstructed images. Subsequent movements were observed by tracking the particles through the sequence of acquisitions at consecutive swelling times. Generally, the centres of the microspheres could be located within ±2 pixels, equivalent to ±0.036 mm, which is smaller than the size of the squares used to indicate the data in Fig. 9. Although the overall patterns of microspheres gradually changed, it was frequently possible to identify 'reference features' such as small clusters that moved in concert, as indicated in Fig. 8.

As noted previously, lateral movements were confined by the minimal clearance between the tablet and the specimen vial used in the present experimental set-up. Nevertheless, even where

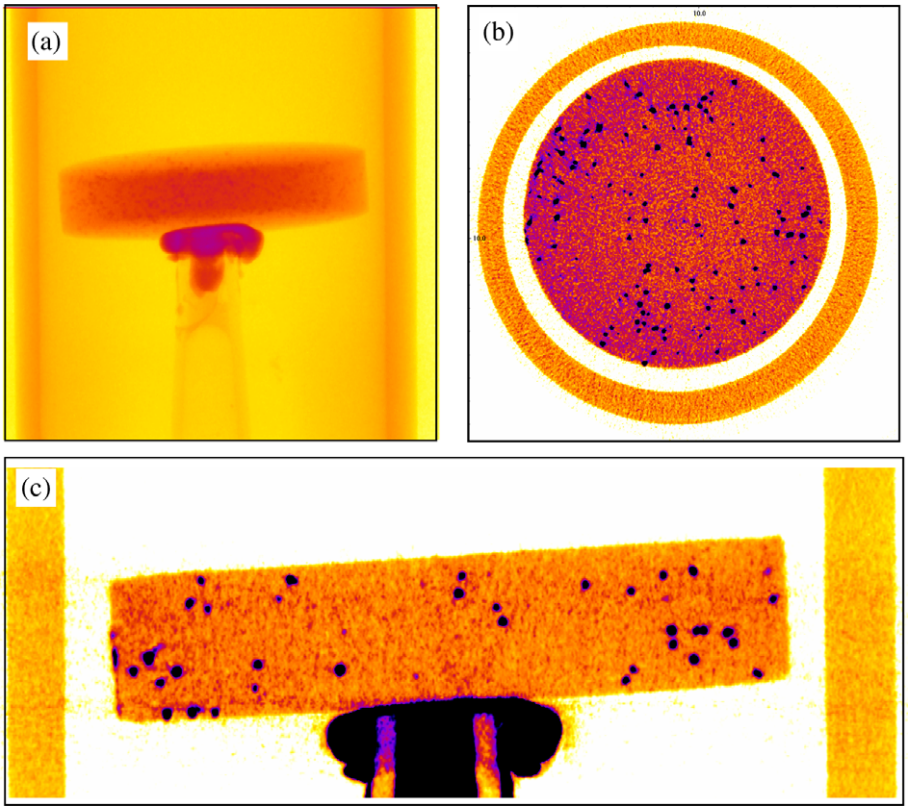

Fig. 7. XμT imaging of dry tablet prior to swelling: (a) typical projection image, (b) reconstructed horizontal (*xy*) slice, (c) reconstructed vertical (*xz*) slice.

lateral movement appeared possible (where there was adequate clearance during the early stages of the experiment), vertical movements still appeared to dominate.

Changes in the vertical positions of selected markers with time are shown in Fig. 9a, plotted against the mid-points of the acquisitions. Swelling of the lower surface initially caused the whole tablet to move upwards. Further swelling caused continued upward movement in the upper part of the tablet. As the lower gel subsequently softened, however, it became impaled on the support, causing downward movement in the lower part of the tablet. This is observable for some of the lower tracks in Fig. 9a. To compensate for this effect, the positions of glass microspheres were calculated relative to a 'reference' marker that was chosen near the middle of the tablet (shown in black, in Fig. 9a). The resulting tracks are shown in Fig. 9b, compared with the extent of the gel as observed by MRI.

3.5. Combined MRI and XμT swelling experiments

The MRI data showed that the hydration fronts moved at constant speed towards the centre of the tablet, where they met after about 3 h. Concurrently, the gel swelled outwards towards the bulk liquid, causing movement of the glass microsphere tracers. Although both sets of data showed roughly similar trends, the MRI results indicated a faster initial increase in thickness and remained systematically ahead of the XμT data for the duration of the experiments. Part of this discrepancy may be due to glass microspheres lagging behind rapidly swelling excipients. It is also possible that the MRI results were affected by dissolved lactose shortening the T_1 of the bulk PBS solution beyond the gel–liquid interface.

A related problem was the possibility of microspheres sinking through the gel, as it swelled and became progressively softer. During the later stages of some experiments, a few tracers near the lower surface of highly swollen tablets were lost from the observations, which can be attributed to the glass spheres falling out of the gel. Nevertheless, this did not appear to be a major problem over the swelling times studied here. Clearly, all the microspheres plotted in Fig. 10a – including near the lower tablet surface – remained within the gel region indicated by MRI.

As expected, the relative (vertical) movements of the glass microspheres depended on their starting positions, with the fastest movements occurring close to the top and bottom surfaces of the tablet. It was more surprising, however, that the movements of all the markers appeared to follow a single relationship of the form:

$$z(t) = z_0 \cdot \{1 + Kt^c\} \quad (5)$$

where z_0 was the (estimated) starting position relative to the reference marker, while K and c were empirical constants ($K = 0.4 \pm 0.02$, $c = 0.7 \pm 0.05$, for the system studied here). This model was used to generate the smooth curves in Fig. 9b. Moreover, the observation that the movements of tracers in different parts of the tablet followed a single model suggested a common process across the tablet.

Significantly, these observations also indicated a modest expansion close to the middle of the tablet within the first two XμT acquisitions (i.e. less than 25 min swelling), including a region of the tablet ahead of the hydration fronts, which appeared dry according to the MRI data. This is shown more clearly by comparing the data from the centre of the specimens, in Fig. 10. The movements of glass microspheres suggested a volumetric expansion of approximately 30% within 1 h, in a region of the tablet that appeared to contain less than 15% w/w water.

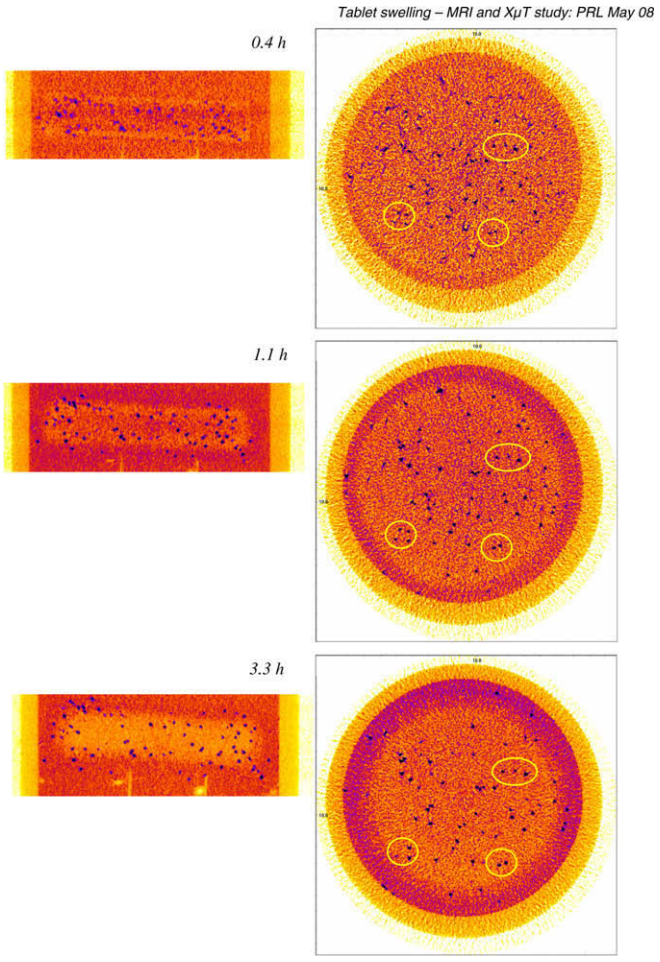

Fig. 8. XμT imaging of tablet during swelling experiments: left – reconstructed vertical (*xz*) slices; right – reconstructed horizontal (*xy*) slices (rings indicate common features observable in the horizontal slices).

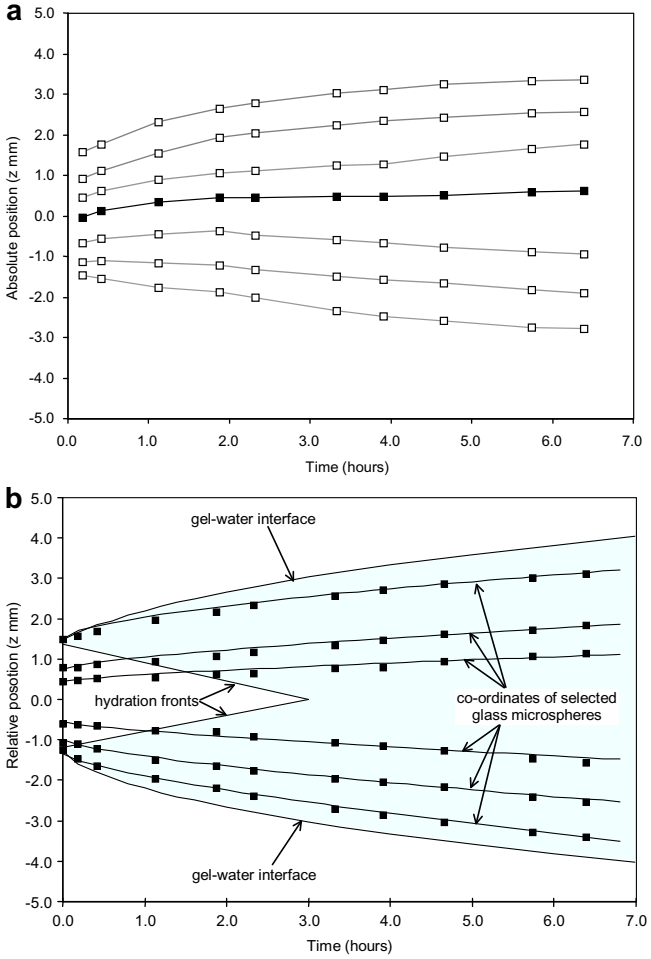

Fig. 9. Tablet swelling observed by tracking glass beads; (a) relative to common co-ordinate system (■ indicates 'reference marker' and the lines are guides for ease of visualisation) and (b) relative to the 'reference' microsphere (the shaded region shows the extent of the gel observed by MRI, and the solid lines represent the relationships described by Eq. (5)).

4. Discussion

The combination of MRI and XμT data suggested that a significant expansion of the tablet core (30% over 1 h) occurred ahead of any observable water ingress, for the formulation studied here. An even larger core expansion (150%) of HPMC tablet cores ahead of observable water ingress was reported previously by Rajabi-Siahboomi et al. using MRI [14], which they attributed to the relaxation of residual (elastic) compaction stress. The difference in magnitude between those results and the present work may be due to tablet composition, size and compaction conditions; Rajabi-Siahboomi et al. used smaller (5 mm diameter) pure HPMC tablets, which were compacted faster and without relaxation at maximum force.

Since the movement of the hydration fronts was the net result of inward diffusion and outward core expansion, the latter effect was not apparent from the MRI results alone in the present work. By contrast, the XμT method was able to observe movements within all parts of the tablet, including those at low hydration levels that could not be observed directly by MRI. This demonstrates the usefulness of the XμT method, in its own right and as a complement to MRI.

It seems unlikely that the core expansion observed in the present work could have been due simply to swelling. Limitations on the sensitivity of MRI observations leave scope for small amounts of water within the tablet core. Nevertheless, the absence of a signal in MRI experiments suggested less than 15% w/w water within the tablet core, which would seem to be insufficient for this level of swelling. Instead, we favour an explanation based on the relaxation

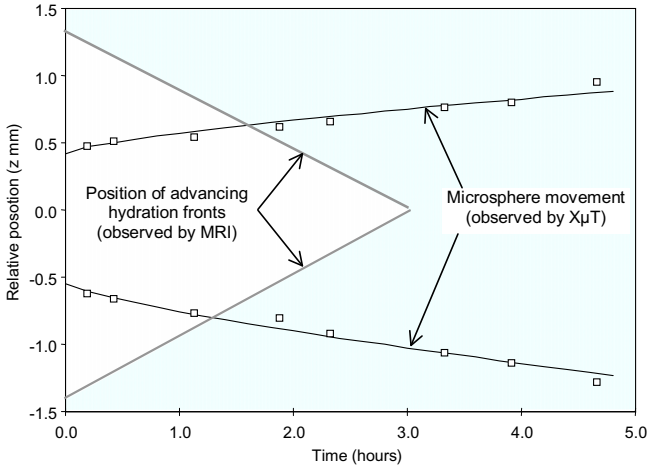

Fig. 10. XμT and MRI observation of tablet core expansion (shaded region shows the extent of the gel observed by MRI).

of residual compaction stress, in line with previous suggestions [14,15,23]. Moreover, recent work [61,62] has suggested that powder compaction causes granule deformation at the nanometre scale, predominantly in the compaction direction; it seems likely that recovery of this during swelling may be responsible for the strong axial expansion.

There may be several possible explanations for how the core expansion was initiated. It is likely that plasticisation of the tablet would permit the relaxation of residual compaction stress. This explanation would imply traces of water ahead of the main hydration front, as proposed previously by Goerke et al. [24], for transport into powdered xanthan. In that model, the liquid hydration front is preceded by vapour penetration, which initiates swelling and is progressively replaced by liquid diffusion as the pores between excipient particles close. Trace levels of water penetrating into polyglycolide was also suggested previously by Milroy et al. [63] to explain the first stage of hydrolysis of this biodegradable polymer. In that work, the ingress of an initially small quantity of water was confirmed by nuclear reaction analysis, although it was undetectable by conventional MRI using spin echo methods.

Alternatively, swelling and softening the outer regions of the tablet may simply remove a mechanical constraint on stress relaxation of the tablet core. This hypothesis would not require (although it would not preclude) water penetration into the tablet core.

Irrespective of the underlying mechanisms, core expansion may be an important mechanism affecting the disintegration and release characteristics of tablets. Although the present work was performed using a gel-forming system, the stress release and core expansion may be more significant with some rapidly dispersing tablets. Further investigations of this are underway and will be reported separately.

5. Conclusions

This paper gives a preliminary account of a novel method for studying the swelling behaviour of tablets, using XμT to observe the movement of glass microsphere markers. Measurements of overall tablet thickness based on tracking the embedded markers compared favourably with MRI results. Moreover, the XμT method revealed expansion within regions of the tablet that contained insufficient water to be observed by the MRI methods used here. This process, which may be due to the release of internal stress, could be an important factor in the disintegration behaviour of tablets.

Acknowledgements

PRL and REC would like to thank Pfizer Ltd. for generous funding and technical support. MDM and LFG wish to thank the EPSRC for financial support and the provision of the MRI spectrometer.

References

[1] R.C. Rowe, Drug Discov. Today 9 (2004) 733–735.
[2] M.E. Aulton, Pharmaceutics: The Science of Dosage Form Design, second ed., Churchill Livingstone, Edinburgh, 2002.
[3] A.M. Hillery, A.W. Lloyd, J. Swarbrick (Eds.), Drug Delivery and Targeting for Pharmacists and Pharmaceutical Scientists, Taylor and Francis, London, 2001.
[4] M.N.V.R. Kumar, N. Kumar, Polymeric controlled drug-delivery systems: perspective issues and opportunities, Drug Dev. Ind. Pharm. 27 (2001) 1–30.
[5] C.D. Melia, Hydrophilic matrix sustained-release systems based on polysaccharide carriers, Crit. Rev. Ther. Drug Carrier Syst. 8 (1991) 395–421.
[6] P. Colombo, R. Bettini, P. Santi, A.P. Nikolaos, Swellable matrices for controlled drug delivery: gel-layer behaviour, mechanisms and optimal performance, Pharm. Sci. Technol. Today 3 (2000) 198–204.
[7] J. Nerurkar, H.W. Jun, J.C. Price, M.O. Park, Controlled-release matrix tablets of ibuprofen using cellulose ethers and carrageenans: effect of formulation factors on dissolution rates, Eur. J. Pharm. Biopharm. 61 (2005) 56–68.
[8] S. Kiortsis, K. Kachrimanis, T. Broussali, S. Malamataris, Drug release from tabletted wet granulations comprising cellulosic (HPMC or HPC) and hydrophobic component, Eur. J. Pharm. Biopharm. 59 (2005) 73–83.
[9] N.K. Ebube, A.B. Jones, Sustained release of acetaminophen from a heterogeneous mixture of two hydrophilic non-ionic cellulose ether polymers, Int. J. Pharm. 272 (2004) 19–27.
[10] D.S. Roy, B.D. Rohera, Comparative evaluation of rate of hydration and matrix erosion of HEC and HPC and study of drug release from their matrices, Eur. J. Pharm. Sci. 16 (2002) 193–199.
[11] R.O. Williams, T.D. Reynolds, T.D. Cabelka, M.A. Sykora, V. Mahaguna, Investigation of excipient type and level on drug release from controlled release tablets containing HPMC, Pharm. Dev. Technol. 7 (2002) 181–193.
[12] M. Levina, A.R. Rajabi-Siahboomi, The influence of excipients on drug release from hydroxypropyl methylcellulose matrices, J. Pharm. Sci. 93 (2004) 2746–2754.
[13] J.C. Richardson, R.W. Bowtell, K. Mäder, C.D. Melia, Pharmaceutical applications of magnetic resonance imaging (MRI), Adv. Drug Deliv. Rev. 57 (2005) 1191–1209.
[14] A.R. Rajabi-Siahboomi, R.W. Bowtell, P. Mansfield, A. Henderson, M.C. Davies, C.D. Melia, Structure and behaviour in hydrophilic matrix sustained-release dosage forms 2. NMR-imaging studies of dimensional changes in the gel layer and core of HPMC tablets undergoing hydration, J. Control. Release 31 (1994) 121–128.
[15] M. Kojima, S. Ando, K. Kataoka, T. Hirota, K. Aoyagi, H. Nakagami, Magnetic resonance imaging (MRI) study of swelling and water mobility in micronized low-substituted hydroxypropylcellulose matrix tablets, Chem. Pharm. Bull. 46 (1998) 324–328.
[16] M. Kojima, H. Nakagami, Investigation of water mobility and diffusivity in hydrating micronized low-substituted hydroxypropyl cellulose, hydroxypropylmethyl cellulose, and hydroxypropyl cellulose matrix tablets by magnetic resonance imaging (MRI), Chem. Pharm. Bull. 50 (2002) 1621–1624.
[17] C.A. Fyfe, A.I. Blazek, Investigation of hydrogel formation from hydroxypropyl methylcellulose (HPMC) by NMR spectroscopy and NMR imaging techniques, Macromolecules 30 (1997) 6230–6237.
[18] C.A. Fyfe, A.I. Blazek-Welsh, Quantitative NMR imaging study of the mechanism of drug release from swelling hydroxypropylmethylcellulose tablets, J. Control. Release 68 (2000) 313–333.
[19] J. Kowalczuk, N. Pislewski, Magnetic resonance imaging study of the swelling kinetics of hydroxypropylmethylcellulose in water, J. Control. Release 80 (2002) 79–86.
[20] J. Kowalczuk, J. Tritt-Goc, N. Pislewski, The swelling properties of hydroxypropyl methylcellulose loaded with tetracycline hydrochloride: magnetic resonance imaging study, Solid State Nucl. Mag. Res. 25 (2004) 35–41.
[21] S. Baumgartner, G. Lahajnar, A. Sepe, J. Kristl, Quantitative evaluation of polymer concentration profile during swelling of hydrophilic matrix tablets using ^{1}H NMR and MRI methods, Eur. J. Pharm. Biopharm. 59 (2005) 299–306.
[22] W.E. Baille, C. Malveau, X.X. Zhu, R.H. Marchessault, NMR imaging of high-amylose starch tablets. 1. Swelling and water uptake, Biomacromolecules 3 (2002) 214–218.
[23] C. Malveau, W.E. Baille, X.X. Zhu, R.H. Marchessault, NMR imaging of high-amylose starch tablets. 2. Effect of tablet size, Biomacromolecules 3 (2002) 1249–1254.
[24] U. Goerke, A.H.L. Chamberlain, E.A. Crilly, P.J. McDonald, Model for water transport into powdered xanthan combining gel swelling and vapour diffusion, Phys. Rev. E 62 (2000) 5353–5359.
[25] J.C.D. Sutch, A.C. Ross, W. Kockenberger, R.W. Bowtell, R.J. MacRae, H.N.E. Stevens, C.D. Melia, Investigating the coating-dependent release mechanism of a pulsatile capsule using NMR microscopy, J. Control. Release 92 (2003) 341–347.
[26] S. Kwiecinski, M. Weychert, A. Jasinski, P. Kulinowski, I. Wawer, E. Sieradzki, Tablet disintegration monitored by magnetic resonance imaging, Appl. Magn. Reson. 22 (2002) 23–29.
[27] B.J. Fahie, A. Nangia, S.K. Chopra, C.A. Fyfe, H. Grondey, A. Blazek, Use of NMR imaging in the optimisation of a compression-coated regulated release system, J. Control. Release 51 (1998) 179–184.
[28] C.D. Melia, A.R. Rajabi-Siahboomi, R.W. Bowtell, Magnetic resonance imaging of controlled release pharmaceutical dosage forms, Pharm. Sci. Technol. Today 1 (1998) 32–39.
[29] M. Ashraf, V.L. Iuorno, D. Coffinbeach, C.A. Evans, L.L. Augsburger, A novel nuclear-magnetic resonance (NMR) imaging method for measuring the water front penetration rate in hydrophilic polymer matrix capsule plugs and its role in drug release, Pharm. Res. 11 (1994) 733–737.
[30] J. Adler, A. Jayan, C.D. Melia, A method for quantifying differential expansion within hydrating hydrophilic matrices by tracking embedded fluorescent microspheres, J. Pharm. Sci. 88 (1999) 371–377.
[31] P.T. Callaghan, Principle of Nuclear Magnetic Resonance Microscopy, Clarendon Press, Oxford, 1995.
[32] B. Blümich, NMR Imaging of Materials, Clarendon Press, Oxford, 2000.
[33] P. Blümler, B. Blümich, R. Botto, E. Fukushima (Eds.), Spatially Resolved Magnetic Resonance, Wiley-VCH, Weinheim, 1997.
[34] M.D. Mantle, A.J. Sederman, Dynamic MRI in chemical process and reaction engineering, Prog. NMR Spectrosc. 43 (2003) 3–60.
[35] P.M. Glover, P.J. McDonald, B. Newling, Stray-field imaging of planar films using a novel surface coil, J. Magn. Reson. 126 (1997) 207–212.

[36] P.J. McDonald, Stray field magnetic resonance imaging, Prog. NMR Spectrosc. 30 (1997) 69–99.
[37] P.J. McDonald, Stray field magnetic resonance imaging: a powerful technique for the quantitative, high resolution imaging of solids, Spectrosc. Eur. 7 (1995) 25–30.
[38] J. Baruchel, J.Y. Buffière, E. Maire, P. Merle, G. Peix, X-ray Tomography in Materials Science, Hermes, Paris, 2000.
[39] S.R. Stock, Recent advances in X-ray microtomography applied to materials, Int. Mater. Rev. 53 (2008) 129–181.
[40] S.R. Stock, X-ray microtomography of materials, Int. Mater. Rev. 44 (1999) 141–164.
[41] A.C. Kak, M. Slaney, Principles of Computerised Tomographic Imaging, IEEE Press, New York, 1988.
[42] S.A. McDonald, M. Preuss, E. Maire, J.Y. Buffiere, P.M. Mummery, P.J. Withers, X-ray tomographic imaging of Ti/SiC composites, J. Microsc. Oxford (Part 2) 209 (2003) 102–112.
[43] E. Masad, V.K. Jandhyala, N. Dasgupta, N. Somadevan, N. Shashidhar, Characterisation of air void distribution in asphalt mixes using X-ray computed tomography, J. Mater. Civil Eng. 14 (2002) 122–129.
[44] E. Maire, A. Fazekas, L. Salvo, R. Dendievel, S. Youssef, P. Cloetens, J.M. Letang, X-ray tomography applied to the characterisation of cellular materials. Related finite element modelling problems, Compos. Sci. Technol. 63 (2003) 2431–2443.
[45] H. Shen, S. Nutt, D. Hull, Direct observation and measurement of fibre architecture in short fibre–polymer composite foam through micro-CT imaging, Compos. Sci. Technol. 64 (2004) 2113–2120.
[46] Y. Nakashima, T. Nakano, K. Nakamura, K. Uesugi, A. Tsuchiyama, S. Ikeda, Three-dimensional diffusion of non-adsorbing species in porous sandstone: computer simulation based on X-ray microtomography using synchrotron radiation, J. Contam. Hydrol. 74 (2004) 253–264.
[47] S.J. Altman, M. Uchida, V.C. Tidwell, C.M. Boney, B.P. Chambers, Use of X-ray absorption imaging to examine heterogenous diffusion in fractured crystalline rocks, J. Contam. Hydrol. 69 (2004) 1–26.
[48] R.E. Guldberg, R.T. Ballock, B.D. Boyan, C.L. Duvall, A.S.P. Lin, S. Nagaraja, M. Oest, J. Phillips, B.D. Porter, G. Robertson, W.R. Taylor, Analysing bone, blood vessels and biomaterials with microcomputed tomography, IEEE Eng. Med. Biol. Mag. 22 (2003) 77–83.
[49] P. Weiss, L. Obadia, D. Magne, X. Bourges, C. Rau, T. Weitkamp, I. Khairoun, J.M. Bouler, D. Chappard, O. Gauthier, G. Daculsi, Synchrotron X-ray microtomography (on a micron scale) provides three-dimensional imaging representation of bone ingrowth in calcium phosphate biomaterials, Biomaterials 24 (2003) 4591–5601.
[50] S.V.N. Jaecques, H. Van Oosterwyck, L. Murara, T. Van Cleynenbreugel, E. De Smet, M. Wevers, I. Naert, J. Vander Sloten, Individualised, micro CT-based finite element modelling as a tool for biomechanical analysis related to tissue engineering of bone, Biomaterials 25 (2004) 1683–1696.
[51] I.C. Sinka, S.F. Burch, J.H. Tweed, J.C. Cunningham, Measurement of density variations in tablets using X-ray computed tomography, Int. J. Pharm. 271 (2004) 215–224.
[52] V. Busignies, B. Leclerc, P. Porion, P. Evesque, G. Couarraze, P. Tchoreloff, Quantitative measurements of localized density variations in cylindrical tablets using X-ray microtomography, Eur. J. Pharm. Biopharm. 64 (2006) 38–50.
[53] Y. Ozeki, Y. Watanabe, S. Inoue, K. Danjo, Comparison of the compression characteristics between new one-step dry-coated tablets (OSDRC) and dry-coated tablets, Int. J. Pharm. 259 (2003) 69–77.
[54] C-Y. Yang, X-Y. Fu, Development and validation of a material-labelling method for powder process characterisation using X-ray computed tomography, Powder Technol. 146 (2004) 10–19.
[55] S.P. Rigby, C.F. Van der Walle, J.H. Raistrick, Determining drug spatial distribution within controlled delivery tablets using MFX imaging, J. Control. Release 96 (2004) 97–100.
[56] I. Aydin, B.J. Briscoe, K.Y. Sanliturk, The internal form of compacted ceramic components: a comparison of a finite element modelling method with experiment, Powder Technol. 89 (1996) 239–254.
[57] B. Eiliazadeh, K. Pitt, B. Briscoe, Effects of punch geometry on powder movement during pharmaceutical tabletting processes, Int. J. Solid Struct. 41 (2004) 5967–5977.
[58] M.D. Hürlimann, Effective gradients in porous media due to susceptibility differences, J. Magn. Reson. 131 (1998) 232–240.
[59] N.L. Thomas, A.H. Windle, A theory of case II diffusion, Polymer 23 (1982) 529–542.
[60] C.D. Melia, A.R. Rajabi-Siahboomi, A.C. Hodsdon, J. Adler, J.R. Mitchell, Structure and behavior of hydrophilic matrix sustained-release dosage forms. 1. The origin and mechanism of formation of gas–bubbles in the hydrated surface-layer, Int. J. Pharm. 99 (1993) 247–252.
[61] P.R. Laity, R.E. Cameron, A small-angle X-ray scattering study of local variations within powder compacts, Powder Technol. 192 (2009) 287–297.
[62] P.R. Laity, R.E. Cameron, A small-angle X-ray scattering study of powder compaction, Powder Technol. 188 (2008) 119–127.
[63] G.E. Milroy, R.W. Smith, R. Hollands, A.S. Clough, M.D. Mantle, L.F. Gladden, H. Huatan, R.E. Cameron, The degradation of polyglycolide in water and deuterium oxide. Part II: nuclear reaction analysis and magnetic resonance imaging of water distribution, Polymer 44 (2003) 1425–1435.